Amphiphilic Layer-by-Layer Assembly Overcoming Solvent Polarity between Aqueous and Nonpolar Media

Minkyung Park,[†,§] Younghoon Kim,[†,§] Yongmin Ko,[†,§] Sanghyuk Cheong,[†] Sook Won Ryu,[‡] and Jinhan Cho*,[†]

[†]Department of Chemical and Biological Engineering, Korea University, Seoul 136-713, Republic of Korea
[‡]Department of Laboratory Medicine, Kangwon National University School of Medicine, Chuncheon-si, Gangwon-do, Republic of Korea

Ⓢ Supporting Information

ABSTRACT: We introduce a general and versatile methodology that allows a facile incorporation of the functional components with completely different chemistry of hydrophilic/hydrophobic properties within nanocomposite films, and furthermore combine a number of the distinctive advantages of traditional electrostatic layer-by-layer (LbL) assembly in aqueous media and covalent LbL assembly in nonpolar media. Our approach, amphiphilic LbL assembly, is based on the high affinity between sulfonic (or phosphonic) acid-functionalized materials in aqueous media and hydrophobic metal oxide (or metal) NPs stabilized by oleic acid

(OA) in nonpolar solvent. For demonstrating the effectiveness of our approach, we show that amphiphilic LbL assembly can be easily applied to the preparation of functional colloid materials allowing the reversible phase transfer between aqueous and nonpolar media, and supercapacitor electrodes with high volumetric capacitance (280 F·cm^{-3} at 10 mV·s^{-1}) using reduced graphene oxide with sulfonic acid moieties and well-defined OA−Fe$_3$O$_4$ NPs.
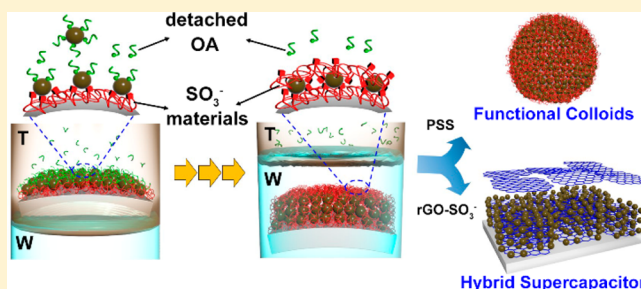
1. INTRODUCTION

The convergence of organic and inorganic materials underpins the development of novel functional materials/films that can significantly improve catalytic, electrical, magnetic, and electrochemical properties.[1−36] Among the various approaches for the preparation of polymer/inorganic nanocomposite films, layer-by-layer (LbL) assembly is potentially the most versatile and well-established method, enabling tailored functionalities, thicknesses, and chemical compositions through complementary interactions between neighboring constituent layers.[1,2,4−15,23−41] To date, LbL assembly has been performed in various solvents, such as water/water,[1,4−10] water/alcohol,[37] alcohol/alcohol,[38,39] alcohol/nonpolar media,[31−35] nonpolar/nonpolar,[40] and mixed solvent[41] systems, but not water/nonpolar media, for the incorporation of desired functional components into the nanocomposites. The utilities, functionalities, and performance of LbL-assembled organic/inorganic nanoparticle (NP) films are strongly dependent on the surface polarity of the outermost layer, the qualities (e.g., crystallinity, size, and shape), and amount of adsorbed functional NPs as well as functionalities of the polymers,[29−34] which are central to the success of most applications. Therefore, high-quality inorganic NPs should be synthesized in nonpolar solvent rather than aqueous media, and a variety of functional components, irrespective of their hydrophobic/hydrophilic properties, should be easily and directly incorporated into the films.

Recently, many research groups have reported that various high-quality, inorganic NPs can be prepared using organic fatty acid ligands (e.g., oleic acid (OA), linoleic acid, or palmitic acid ligands) in nonpolar media.[42,43] For successive LbL assembly in connection with other organic materials, such as polymers, these hydrophobic NPs generally require a phase transfer from a nonpolar solvent to an aqueous medium using a ligand exchange reaction[44,45] or a nanocontainer, such as block copolymer micelles,[46] composed of a hydrophobic core and hydrophilic corona shell. However, in this electrostatic LbL approach, the electrostatic repulsion between the resulting aqueous NPs (or the NP-incorporated nanocontainer) with the same charges considerably reduces the packing density of each NP layer (or nanocontainer layer), and the loading amount of functional NPs has a strong influence on the performance of inorganic NP-based nanocomposite films.

As another approach for incorporating hydrophobic materials into LbL-assembled films, Kong et al. reported that water-soluble anionic polyelectrolytes (PEs) could be grafted onto the surfaces of hydrophobic materials via surface-initiating atom transfer radical polymerization and that the resulting charged PE-grafted hydrophobic components could be LbL assembled using oppositely charged PEs in an aqueous solvent.[47] Additionally, Tetty et al. reported that the electrostatic LbL

assembly of nonwater-soluble materials (i.e., carbon black with a negative charge and alumina with a positive charge) was performed with the aid of charge-inducing surfactant in toluene.[40] However, a few attempts have been made at the LbL assembly of the well-defined hydrophobic NPs (metal or metal oxide NPs) in nonpolar media and the NH_2-polymer in polar organic media.[31−36] For example, it was reported that hydrophobic Au NPs dispersed in nonpolar media could be LbL-assembled using an amine-functionalized polymer (i.e., NH_2-polymer).[33,34] Our groups also reported that 2-bromo-2-methylpropionic acid (BMPA)-stabilized NPs (i.e., BMPA−CdSe@ZnS and BMPA−Fe_3O_4 NPs) or OA-stabilized metal (or transition metal oxide NPs) dispersed in toluene could be LbL-assembled using an amine-functionalized dendrimer (i.e., NH_2-dendrimer) in ethanol.[31,32,35,36] These previous approaches, despite the high loading amount of the well-defined NPs onto the polymer layer, have a partial disadvantage in that water-soluble/dispersible materials (i.e., PEs, biomaterials, and electrostatically charged carbon materials) cannot be directly LbL-assembled with a variety of high-quality, functional inorganic metal and metal oxide NPs dispersed in nonpolar media. This drawback can be a critical obstacle to prepare LbL-assembled nanocomposite films that can exhibit the unique functionalities of their hydrophilic and hydrophobic constituents. For example, in the case of preparing functional colloids allowing for reversible dispersion in aqueous and nonpolar media using the previously reported approach,[36] additional adsorption processes for the insertion of alcohol-soluble hydrogen-bonding polymer layers are required, and careful steps should be taken to prevent the colloidal aggregation occurring during the adsorption of the hydrogen-bonding polymer layers. Additionally, these approaches[31−36] have difficulties in preparing the two-dimensional (2D)-nanosheet/inorganic NP nanocomposite films in organic media (i.e., alcohol, toluene or hexane) because of their poor dispersion stability and stacking phenomena. Although it was reported that highly dispersible graphene oxide (GO) sheets could be prepared in organic media by introducing organic moieties with long chains onto the surface of the GO sheet,[48−50] the formed GO sheets had no interaction with the surface of the hydrophobic NPs, such as OA-NPs, for the buildup of LbL-assembled films. Thus, the 2D-sheet functional films, such as GO sheet/metal oxide nanocomposites, which can be used as a supercapacitor electrode in energy storage devices, have mainly been prepared via electrostatic LbL assembly, thus inducing a relatively low loading amount of metal oxide NPs.[51,52]

In this regard, one of the most significant challenges is exploiting the direct assembly of electrostatically charged materials (i.e., PEs and GO sheets) and hydrophobic NPs. This unique LbL assembly approach could incorporate and integrate more diverse functional materials within the nanocomposite multilayers and significantly increase the packing density of well-defined NPs while simultaneously permitting a wide variety of potential applications in aqueous, polar, or nonpolar organic media.

Here, we introduce a general and versatile approach for preparing functional nanocomposite multilayers via the consecutive adsorption of hydrophobic metal or metal oxide NPs stabilized by OA ligands and electrostatically charged components onto substrates. The strategy, amphiphilic LbL assembly using sulfonic acid (SO_3^-) (or phosphonic acid, PO_3^{2-})-functionalized components, is based on the high affinity between the surface of metal oxide (or metal) NPs in nonpolar

solvent and the SO_3^- groups of PEs in aqueous solution. In this case, OA-stabilized NPs (OA-NPs) were used as hydrophobic metal or metal oxide NPs because it was reported that OA ligands can be widely employed for the preparation of various NPs, ranging from metal to binary or perovskite-type metal oxide NPs, and that the carboxylate ions of OA ligands loosely bound to the surface of metal or metal oxide NPs can be easily replaced by other ligands containing a higher-affinity group with NPs.[53−56]

Although hydrophilic/hydrophobic multilayers can be prepared by a solvent medium-independent process that includes spray-assisted LbL assembly,[57] such a process should also be based on the high affinity between two different component layers. Otherwise, hydrophilic (or hydrophobic) components may not be uniformly adsorbed onto a sublayer composed of hydrophobic (or hydrophilic) components due to unfavorable interfacial interactions and will furthermore be easily removed by the same deposition solution. Thus, the variety of hydrophilic/hydrophobic multilayers shown in our approach is realized not only by process tools but also by unique interfacial interactions.

Our approach highlights the fact that a variety of functional components, ranging from water-soluble/dispersible materials to hydrophobic NPs, can be easily and directly incorporated within multilayer films without the additional surface modification of pristine NPs or the insertion of additional polymer layers. Another notable advantage of amphiphilic LbL assembly is that the amount of adsorbed hydrophobic NPs can be controlled by the ionic strength of the preadsorbed PE layer, and their packing density is greater than 50%. These findings imply that a variety of functional layers with extremely different hydrophilic/hydrophobic properties can be easily integrated into the nanocomposite multilayers, and our approach can include the respective advantages of the aqueous and nonpolar solvent-based LbL assemblies reported to date.

Based on the unique properties of amphiphilic LbL-assembly, we demonstrate that our approach can be effectively applied to the preparation of functional colloids, thus allowing for a reversible phase transfer between aqueous and nonpolar media. Furthermore, we demonstrate that when the (rGO−SO_3^-/OA−Fe_3O_4 NP)$_n$ nanocomposite films are applied to supercapacitor electrodes, their energy density can be significantly enhanced within the limited volume of the electrode due to the high packing density of well-defined Fe_3O_4 NPs.

Because a variety of OA-stabilized metal or metal oxide NPs (e.g., OA−Fe_3O_4, OA−TiO_2, OA−MnO, OA−Ag NPs) dispersed in nonpolar (e.g., toluene or hexane) or polar organic (e.g., tetrahydrofuran (THF) or chloroform) media can be directly LbL-assembled using SO_3^- or PO_3^{2-} group-based materials (e.g., poly(4-sodium, styrenesulfonic acid) (PSS), poly(vinyl phosphonic acid) (PVPA), poly(3,4-ethylenedioxythiophene):poly(styrenesulfonate) (PEDOT:PSS), or reduced graphene oxide nanosheets containing SO_3^- groups (rGO−SO_3^-)) in aqueous media, our strategy can provide a basis for developing and designing functional nanocomposite films for applications, such as energy storage devices, magnetically retrievable catalytic colloids in the petrochemical industry, and electronic devices.

2. EXPERIMENTAL SECTION

Materials. PSS (M_w = 70 000, Aldrich) of 1 mg·mL^{-1} in aqueous solution was used as an anionic polyelectrolyte. OA−Ag,[58] OA−Fe_3O_4,[42,59] OA−MnO,[35] OA−TiO_2 NPs,[60] rGO−SO_3^-,[61,62] and

rGO−NH$_3^+$ [63] were prepared as previously reported by other research groups. Additional experimental details are given in the Supporting Information.

3. RESULTS AND DISCUSSION

In this study, OA−Fe$_3$O$_4$ NPs with a diameter of approximately 8.6 nm were prepared in toluene and sulfonic acid functionalized materials, including poly(sodium 4-styrenesulfonate) (PSS), and water and were used for the buildup of LbL nanocomposite films (Scheme 1). First, a high affinity between

Scheme 1. Schematic Illustration of the Amphiphilic LbL Growth of Sulfonic Acid-Functionalized Component/OA−Fe$_3$O$_4$ NP Multilayers
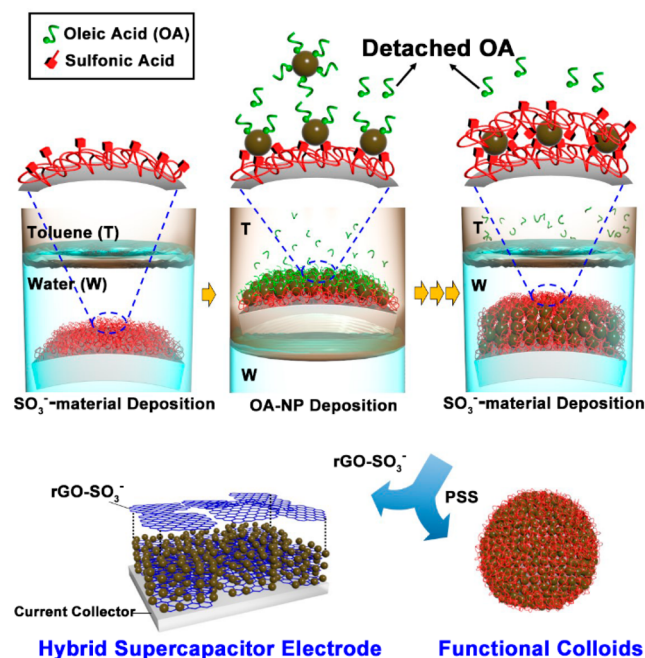
the SO$_3^-$ groups of PSS and the oxide surface of the OA−Fe$_3$O$_4$ NPs was demonstrated using FTIR spectroscopy. The FTIR spectrum of PSS displayed prominent absorption peaks originating from aromatic rings (at 1500 cm^{-1}) and SO$_3^-$ stretching vibrations (at 1009, 1040, 1128, and 1190 cm^{-1}). Additionally, the COO$^-$ asymmetrical stretching peaks (1525 cm^{-1}) indicated that the OA ligands were bound to the surfaces of the Fe$_3$O$_4$ NPs (see Supporting Information, Figure S1). Zhang et al. reported that COO$^-$ asymmetrical stretching bands appeared instead of the COOH stretching band from carboxyl groups when the OA ligands were bound to the surfaces of Fe$_3$O$_4$ NPs.[64,65] These distinctive absorption peaks from SO$_3^-$ and COO$^-$ stretching were observed in the PSS/OA-Fe$_3$O$_4$ NP multilayers. As the PSS layer was further adsorbed onto the OA−Fe$_3$O$_4$ NP-coated film as a function of the deposition time, the absorption peak intensity of the COO$^-$ stretching gradually decreased and the intensity of the −SO$_3^-$ group peak of PSS increased (Figure 1a). Additionally, the alternating deposition of PSS and OA−Fe$_3$O$_4$ NPs produced inversely correlated changes in the peak intensities of the SO$_3^-$ and COO$^-$ stretching frequencies (Figure 1b) and resultantly induces the vertical growth of PSS/OA−Fe$_3$O$_4$ NP multilayers (see Supporting Information, Figure S2). These phenomena indicate that the SO$_3^-$ groups in the PSS are adsorbed onto the surface of Fe$_3$O$_4$ NPs via coordination bonding after OA ligand
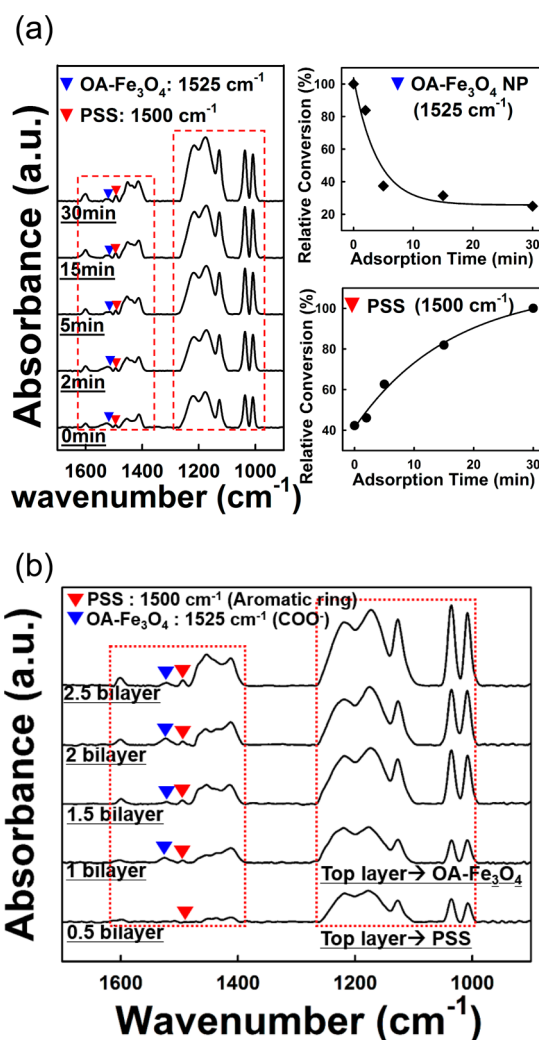
Figure 1. (a) ATR-FTIR spectra of (PSS/OA−Fe$_3$O$_4$ NP/PSS) film as a function of the adsorption time of PSS onto the outermost OA−Fe$_3$O$_4$ NP layer-coated films. The relative conversion rate was calculated by comparing the ATR-FTIR absorption peak area of the COO$^-$ group (at 1525 cm^{-1}) of the OA ligand and the SO$_3^-$ group (at 1500 cm^{-1}) of PSS as a function of PSS adsorption time. (b) ATR-FTIR spectra of (PSS/OA−Fe$_3$O$_4$ NP)$_n$ multilayers as a function of the bilayer number.

replacement. Yee et al. reported that the sulfonic acid groups of various alkanesulfonic acid surfactants in organic media are coordinately bonded with the Fe^{3+} site at the surface of amorphous iron oxide NPs; they therefore act as monodentate ligands.[66] Another example was demonstrated by Kim et al., in which nanocomposites composed of sol−gel processed vanadium oxide (s-VO$_x$) and PSS formed −V−O−SO$_2$.[67] In contrast, Polito et al. reported that sulfonic acid moieties of organic compounds in organic media serve as bidentate ligands, binding to Fe via two O atoms when they are adsorbed onto the surface of OA-Fe$_3$O$_4$ NPs.[68] Although we do not know exactly whether the coordination bond between the SO$_3^-$ and Fe sites is monodentate or bidentate due to the contradictory results reported by other research groups,[66,68] in view of polymer ligands containing a number of sulfonic acid groups, it is clear that PSS serves as a multidentate ligand, which is different from other organic ligands containing one sulfonic acid (i.e., alkanesulfonic acid ligand) or carboxylic acid (i.e., oleic acid ligand) group. This multidentate ligand can provide
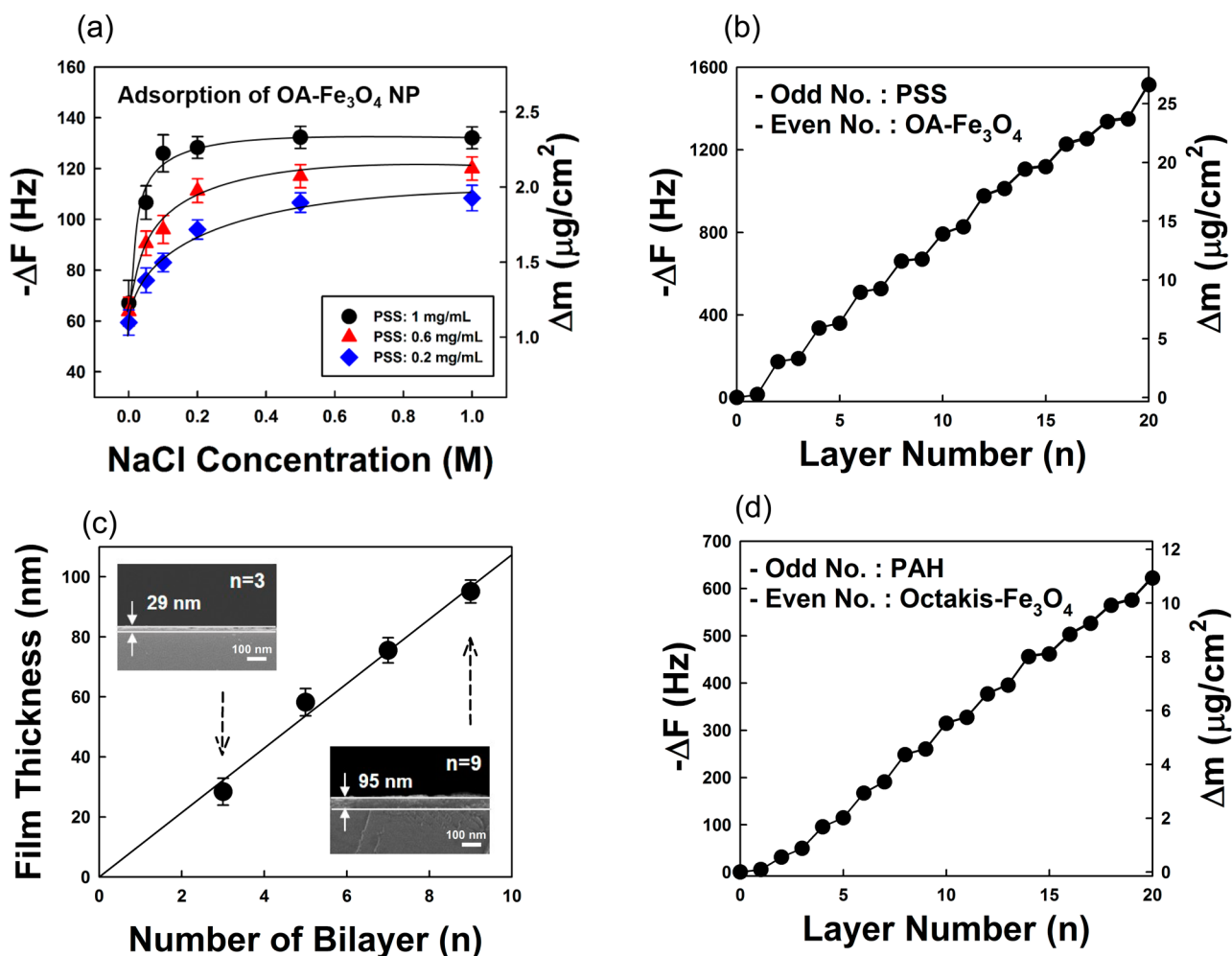
Figure 2. (a) Frequency and mass change of the adsorbed OA−Fe_3O_4 NPs as a function of ionic strength of the PSS solution. For this measurement, the ionic strength of the PSS solution was increased from 0 to 1 M NaCl, and the adsorption time of OA−Fe_3O_4 NPs onto the outermost PSS layer was fixed at 45 min. (b) Frequency and mass change of PSS/OA−Fe_3O_4 NP multilayers as a function of the layer number. The solution concentration of 0.2 M NaCl PSS and OA−Fe_3O_4 NP was adjusted to be 1 and 10 mg·mL^{-1}, respectively. (c) The total film thicknesses of the (PSS/ OA−Fe_3O_4 NP)$_{n=3,5,7 \text{ and } 9}$ multilayers measured from the cross-sectional SEM images. Deposition conditions were identical to those of (b). (d) Frequency and mass change of PAH/anionic Fe_3O_4 NP multilayers as a function of the layer number. In this case, the solution concentration of 0.2 M NaCl PAH and 0.3 M NaCl anionic Fe_3O_4 NP were 1 and 10 mg·mL^{-1}, respectively.

enhanced coordination interactions due to the cooperative, amplifying effect of multiple binding sites. Therefore, the ligand exchange between PSS (multidentate ligand) and OA (monodentate ligand) can be driven by an entropy increase in the system and by a higher binding affinity for Fe_3O_4 NPs than for the OA ligand.

In line with our FTIR results, our results imply that OA ligands loosely bound to the surface of Fe_3O_4 NP can be replaced by the SO_3^- groups of PSS and that the polymers containing stronger acid groups than carboxylic acid groups of OA ligands can also have a higher affinity for iron oxide NPs than weak acid groups, such as COO^-. This possibility was supported by the results that the water-soluble PVPA, which has the stronger acid groups (i.e., phosphonic acid) than COO^- groups of OA ligands, could be LbL-assembled with OA−Fe_3O_4 NPs in nonpolar media (see Supporting Information, Figure S3).

Based on these adsorption properties, the amount of OA-Fe_3O_4 NPs adsorbed onto the PSS layer prepared at different ionic strengths (i.e., concentration of NaCl) and concentrations (i.e., 0.2, 0.6, and 1 mg·mL^{-1}) was quantitatively monitored using frequency changes measured from a quartz crystal microbalance (QCM) coated with poly(allylamine hydrochloride) (PAH) (see Figure 2a).

First, the loading amount of OA−Fe_3O_4 NPs (10 mg·mL^{-1}) was rapidly saturated with increasing solution concentration and the ionic strength of the PSS solution. In particular, the $-\Delta F$ (or mass change, Δm) of the 0 M NaCl PSS (1 mg·mL^{-1}) and OA−Fe_3O_4 NP (10 mg·mL^{-1}) layers were 25 ± 7 (Δm, ~441 ng·cm^{-2}) and 67 ± 13 Hz (Δm, ~1183 ng·cm^{-2}), respectively (the standard deviation of $-\Delta F$ was obtained from repeated measurements of the same layer). However, when the ionic strength of the PSS solution was increased from 0 to 0.2 M NaCl, the $-\Delta F$ (or Δm) of each OA−Fe_3O_4 NP and PSS also significantly increased up to 132 ± 3 Hz (Δm, ~2332 ng· cm^{-2}) and 42 ± 9 Hz (Δm, ~742 ng·cm^{-2}), respectively. A further increase in the ionic strength of the PSS solution (1 mg· mL^{-1}) above 0.2 M NaCl did not increase the adsorbed amount of OA−Fe_3O_4 NPs; however the adsorbed amount of PSS increased continuously with increasing ionic strength (see Supporting Information, Figure S4). In the case of consecutively depositing 0.2 M NaCl PSS and OA−Fe_3O_4 NPs,

regular and vertical growth of (PSS/OA−Fe$_3$O$_4$ NPs)$_n$ multilayers was observed, as shown in Figure 2b. The thickness of the nanocomposite films prepared using 0.2 M NaCl PSS, which increases linearly with the bilayer number, was measured using SEM images (Figure 2c). These results indicate that the adsorbed amount of hydrophobic NPs dispersed in nonpolar solvent is significantly influenced by the adsorption states of the preadsorbed PSS as a strong PE with fixed charge densities. More specifically, an increase in the ionic strength of PSS changes the chain conformation from a relatively extended structure to a loop and/or coil structure because of the decrease in the electrostatic repulsion from the groups with the same charged in the strong PE chains, which generates a number of free ionic binding sites on the PSS surface.[69] Thus, this adsorption state of the previously adsorbed PSS layer can induce a larger amount of adsorbing OA−Fe$_3$O$_4$ NPs in the next layer. However, even if the PSS layer thickness (i.e., adsorbed amount) is increased to an ionic salt concentration greater than 0.2 M NaCl, the hydrophobic NPs have considerable difficulty in infiltrating deeply within the hydrophilic PSS layer, and therefore, the OA−Fe$_3$O$_4$ NPs are adsorbed onto only the surface of the outermost PSS layer without strong interdiffusion,[44,70,71] as observed in conventional electrostatic LbL assembly. As a result, the amount of OA−Fe$_3$O$_4$ NPs adsorbed onto the PSS layer with an ionic strength of 0.2 M NaCl reached a plateau despite further increases in the ionic strength (see Figure 2a).

In contrast, the pH of the PSS solution has little effect on the adsorbed quantity of PSS and OA−Fe$_3$O$_4$ NPs because strong polyelectrolytes with SO$_3^-$ groups have almost fixed charge densities across a broad pH range. To confirm this phenomenon, we investigated the number of (0.2 M NaCl PSS/OA−Fe$_3$O$_4$ NP)$_n$ multilayers adsorbed upon increasing the pH of a 0.2 M NaCl PSS solution from 3 to 9. The UV−vis absorbance (at 225 nm) of the (0.2 M NaCl PSS/OA−Fe$_3$O$_4$ NP)$_n$ multilayers prepared at a pH of 6 was almost identical to that of the multilayers prepared from PSS at pH values of 3 and 9 (see Supporting Information, Figure S5).

The magnetic properties of the resulting (0.2 M NaCl PSS/OA−Fe$_3$O$_4$ NP)$_n$ multilayers were also examined by superconducting quantum interference device magnetometry (SQUID). These nanocomposite films based on well-defined Fe$_3$O$_4$ NPs exhibited typical superparamagnetic properties, displaying reversible magnetization curves without coercivity, remanence, or hysteresis at room temperature (see the Supporting Information, Figure S6).[70−74] However, at liquid helium temperature (T = 5 K), the thermally activated magnetization flipping properties of the (0.2 M NaCl PSS/OA−Fe$_3$O$_4$)$_n$ nanocomposite films demonstrated frustrated superparamagnetic properties. Another notable phenomenon is that amphiphilic LbL assembly can easily realize a high packing density of well-defined hydrophobic NPs despite the introduction of an electrostatically charged PE layer, as previously noted. For more evidence demonstrating this advantage, the packing density of 8.6 nm OA-Fe$_3$O$_4$ NPs adsorbed onto 0.2 M NaCl PSS layers (1 mg·mL^{-1}) was calculated using the volume size (∼3.33 × 10^{-19} cm^3), the mass density (∼5 g·cm^{-3}) of a single OA−Fe$_3$O$_4$ NP, and the number density per unit area (∼1.34 × 10^{12} cm^{-2}) of the OA−Fe$_3$O$_4$ NP array. In this case, the 2D and 3D packing densities of OA−Fe$_3$O$_4$ NPs per layer were calculated to be approximately 77.8% and 52%, respectively (calculation details are provided in Supporting Information). However, when 10

bilayered films (i.e., (OA−Fe$_3$O$_4$ NP/PSS)$_{10}$/PAH-coated QCM electrode) were thermally dried at 120 °C for 5 h after the OA−Fe$_3$O$_4$ NP layer was deposited, the −ΔF (or Δm) of the multilayer was decreased slightly from 1514 ± 3 Hz to 1501 ± 7 Hz. The 0.84% decrease in Δm after thermal annealing is mainly caused by the removal of residual aqueous solvents within the PSS/PAH multilayers because toluene is more volatile than water. As a result, the 3D and 2D packing densities of the OA−Fe$_3$O$_4$ NPs after eliminating residual solvent were approximately 51.6% and 77.5%, respectively, which is nearly identical to the packing densities of the OA−Fe$_3$O$_4$ NP layer before thermal annealing and is close to the maximum 3D packing density (≈ 64%)[75] for a randomly close-packed particle layer. In the case of (PVPA/OA−Fe$_3$O$_4$ NP)$_n$ multilayers, the 2D and 3D packing densities of OA−Fe$_3$O$_4$ NPs were calculated to be 69% and 46%, respectively (see Supporting Information, Figure S7). On the other hand, the packing density of electrostatic NPs per layer is typically below 30% (we could not confirm whether the packing densities described in previous papers are 2D or 3D packing densities).[76−78] Although increasing the ionic strength (i.e., increasing the ionic salt concentration) or pH of the aqueous NP solution can increase the number of NPs absorbed onto the oppositely charged layer, a decrease in the electrostatic repulsion between NPs with the same charge induces the aggregation of NPs in aqueous solution and may deteriorate the quality of the nanocomposite film.

To confirm these possibilities, OA−Fe$_3$O$_4$ NPs dispersed in toluene were first phase-transferred to aqueous media using negatively charged octakis ligands. After the phase transfer, the NaCl concentration was increased from 0 to 0.7 M in an anionic Fe$_3$O$_4$ NP (i.e., octakis-Fe$_3$O$_4$ NP) aqueous solution, and the anionic Fe$_3$O$_4$ NPs started to aggregate above 0.3 M NaCl (see Supporting Information, Figure S8). Therefore, to prevent NP aggregation, 0.3 M NaCl was added to the anionic Fe$_3$O$_4$ NP solution, and then, they were electrostatically LbL-assembled with cationic poly(allylamine hydrochloride) (PAH).

However, despite the addition of the ionic salt, the amount of anionic Fe$_3$O$_4$ NPs adsorbed in the (0.2 M NaCl PAH/0.3 M NaCl anionic Fe$_3$O$_4$ NP)$_n$ multilayers was considerably lower than that of the OA−Fe$_3$O$_4$ NPs in the (PSS/OA−Fe$_3$O$_4$ NP)$_n$ films (Figure 2d). These results imply that our approach has a clear advantage in terms of increasing the packing density of functional NPs compared to electrostatic LbL assembly.

To better understand the adsorption state shown in the (PSS/OA−Fe$_3$O$_4$ NPs)$_n$ multilayers, the changes in the surface wettability of the (PSS/OA−Fe$_3$O$_4$ NPs)$_n$ nanocomposite film were investigated according to the alternating deposition of anionic PSS and hydrophobic NPs (Figure 3a). The surface wettability of the sequentially adsorbed polymer and/or NP layers is sensitive to the chemical composition of the adsorbed materials, the hydrophilicity of their functional groups, the level of interpenetration of the outermost layer by segments of the previously adsorbed layer, and the surface coverage of the outermost layer.[79] Therefore, if the hydrophobic NPs are loosely packed onto the polymer layer and/or infiltrated into the PE layer, all of the water contact angles measured on the NP and polymer layers are nearly constant, without any evident periodic oscillation. These phenomena have been observed in electrostatic LbL-assembled polymer/inorganic NP films based on the dipping solution process.[80] However, in the case of amphiphilic LbL assembly, the alternating deposition of anionic PSS (containing 0.2 M NaCl) and hydrophobic NPs led to

(a)

(a)

(b)

(b)
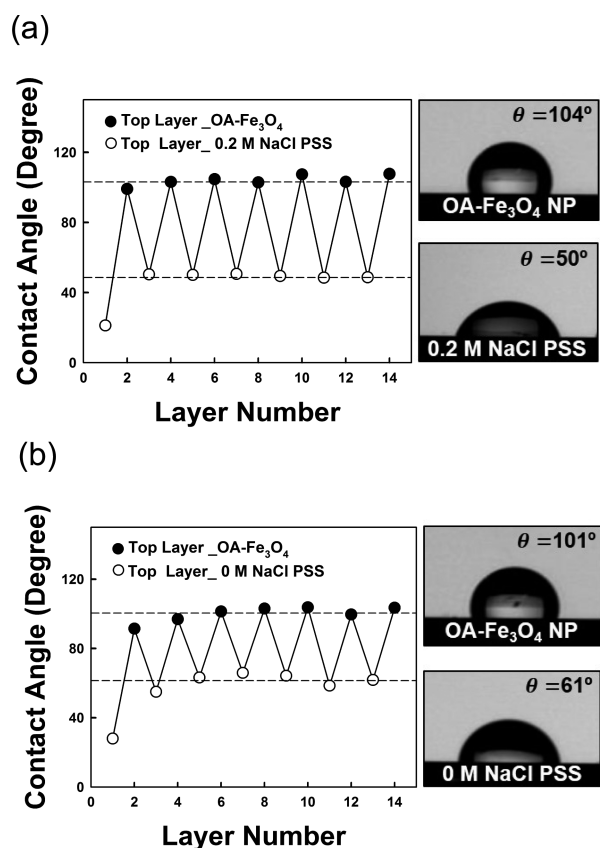
Figure 3. Water contact angles measured from (a) (0.2 M NaCl PSS/ OA−Fe$_3$O$_4$ NP)$_n$ and (b) (0 M NaCl PSS/OA−Fe$_3$O$_4$ NP)$_n$ multilayers. In this case, odd and even numbers indicate the layers deposited with the PSS (1 mg·mL^{-1}) and OA−Fe$_3$O$_4$ NP (10 mg· mL^{-1}) layer, respectively.

large periodic oscillations from 49°−53° (for PSS as a top layer) to 102°−108° (for OA−Fe$_3$O$_4$ NPs as a top layer) in the water contact angle on the resulting multilayer film (Figure 3a).

These results support the notion that the densely packed outermost OA−Fe$_3$O$_4$ NP (or PSS) layers effectively screen chemical and physical properties of the PSS sublayer (or OA− Fe$_3$O$_4$ NPs) as discussed earlier. In the case of (0 M NaCl PSS/ OA−Fe$_3$O$_4$ NP)$_n$ multilayers, the water contact angles were periodically changed from 55°−65° (for PSS as a top layer) to 97°−103° (for OA−Fe$_3$O$_4$ NPs as a top layer) (Figure 3b). This decrease in the oscillations of the water contact angle implies that the chemical and/or physical properties of the outermost layer (i.e., PSS or OA−Fe$_3$O$_4$ NPs) are partially influenced by those of the sublayer due to incomplete surface coverage.

Furthermore, these extreme changes in the surface wettability imply that amphiphilic LbL assembly can be effectively used for colloidal applications that require high dispersion stability in aqueous and/or nonpolar media. To investigate these possibilities, the (PSS/OA−Fe$_3$O$_4$ NP)$_n$ multilayers were consecutively deposited onto SiO$_2$ colloids. As shown in Figure 4a, the solution dispersion of (PSS/OA−Fe$_3$O$_4$ NP)$_n$ multi-layer-coated colloids in aqueous and toluene phases was strongly dependent on the properties of the outermost layer. The observed results not only demonstrate the LbL growth of the PSS/OA−Fe$_3$O$_4$ NP multilayer films but also suggest that the dispersion stability of the colloidal nanocomposites can be
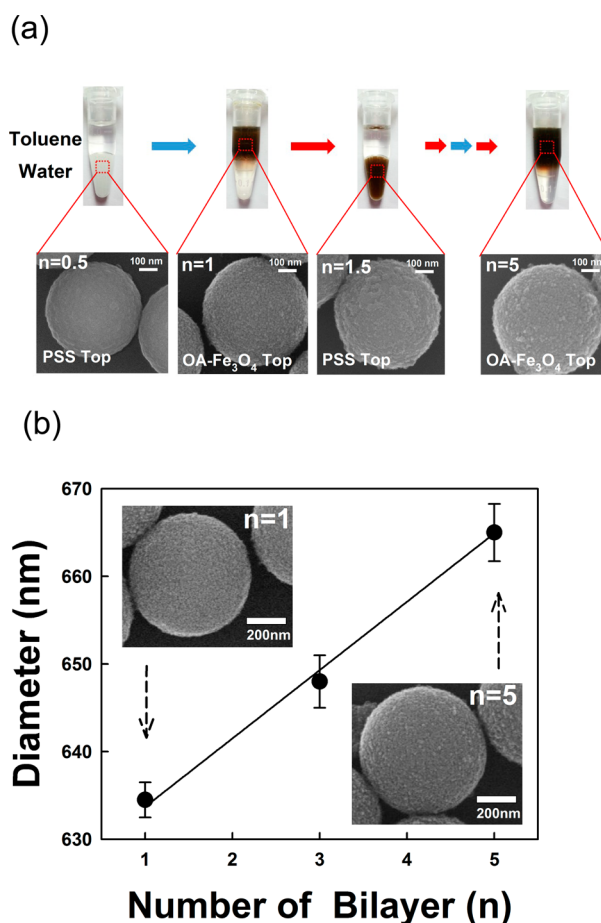
Figure 4. (a) Photographic and SEM images of (0.2 M NaCl PSS/ OA−Fe$_3$O$_4$ NP)$_n$ multilayer-coated cationic SiO$_2$ colloids. The bare SiO$_2$ colloids with a diameter of about 600 nm were used for amphiphilic LbL-assembly. (b) The size change of (0.2 M NaCl PSS/ OA−Fe$_3$O$_4$ NP)$_n$ multilayer-coated colloids with increasing bilayer number (n). The solution concentration of 0.2 M NaCl PSS and OA− Fe$_3$O$_4$ NP was adjusted to be 1 and 10 mg·mL^{-1}, respectively.

dramatically altered by the outermost layer on the nanometer scale.

However, the amphiphilic LbL assembly exhibited a notable difference in the amount of adsorbed functional components between the flat and colloidal substrates. For example, the diameter of the (PSS/OA−Fe$_3$O$_4$ NP)$_n$ multilayer-coated colloids increased from approximately 600 to 665 nm without any colloidal aggregation as shown in SEM images when the bilayer number (n) of multilayers was increased from 0 to 5 (Figure 4b). In this case, the thickness per bilayer deposited onto the colloidal substrates was measured to be approximately 6.5 nm, which was much smaller than that of the PSS/OA− Fe$_3$O$_4$ NP bilayer obtained on the flat substrates despite using the same solution concentrations and deposition times (i.e., a bilayer thickness of approximately 10 nm). This difference in the bilayer thicknesses may be caused by the presence of a relatively large amount of residual solvent adsorbed onto the outermost layer. That is, when depositing the hydrophilic PSS onto the colloidal substrate without a drying procedure after the deposition and successive washing process of the hydrophobic OA−Fe$_3$O$_4$ NPs, the formation of a thin layer of nonpolar (or water) solvent on the outermost OA−Fe$_3$O$_4$ (or PSS) layer can partially disturb the adsorption of water-

17218

dx.doi.org/10.1021/ja509168g | J. Am. Chem. Soc. 2014, 136, 17213−17223
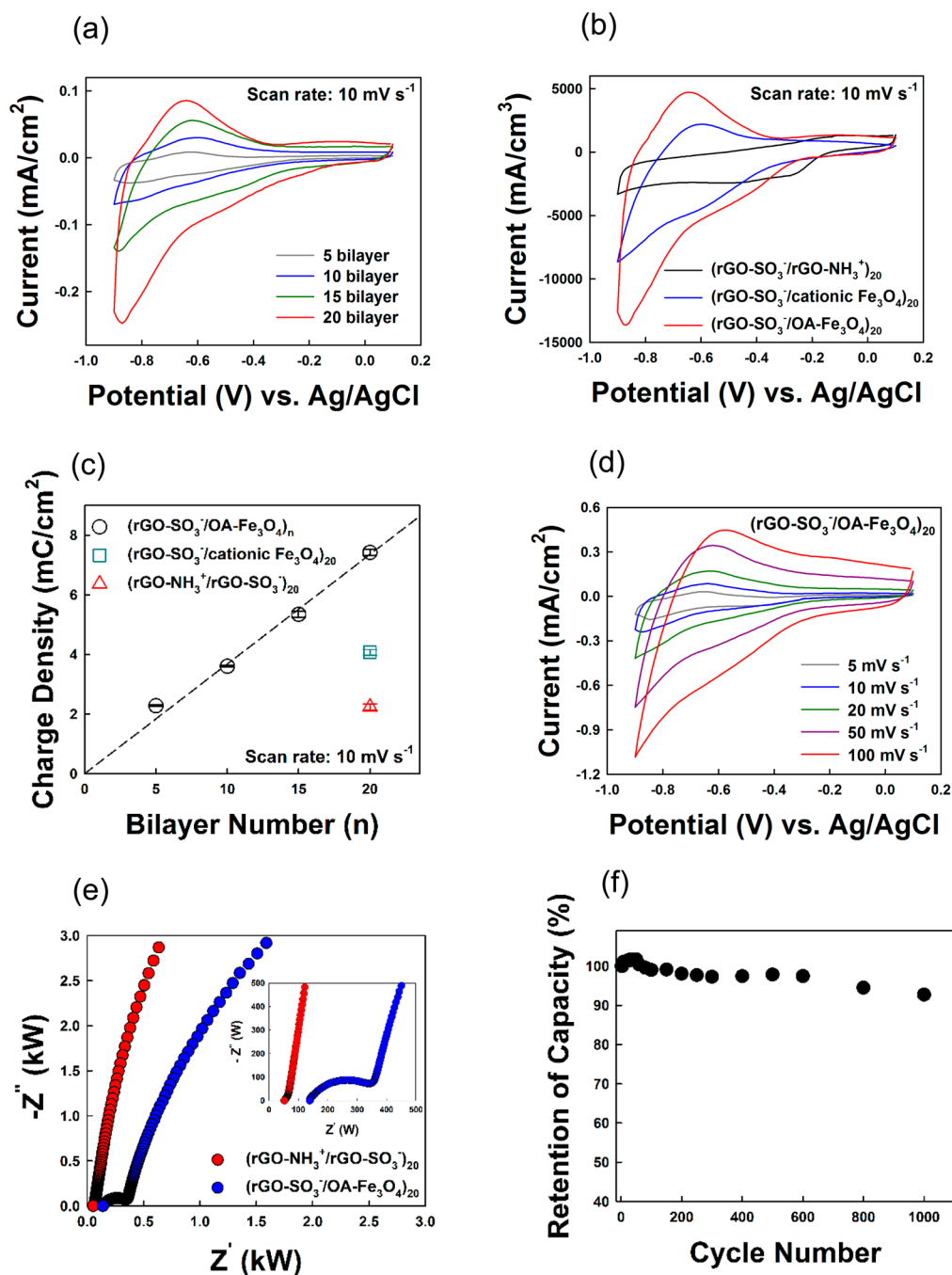
Figure 5. CVs of the LbL-assembled (a) $(rGO-SO_3^-/OA-Fe_3O_4\ NP)_{n=5,10,15,\ and\ 20}$ and (b) $(rGO-SO_3^-/OA-Fe_3O_4\ NP)_{20}$, the $(rGO-SO_3^-/cationic\ Fe_3O_4\ NP)_{20}$, and the $(rGO-NH_3^+/rGO-SO_3^-)_{20}$ electrodes at a scan rate of 10 mV·s^{-1}. (c) Total integrated charges of the $(rGO-SO_3^-/OA-Fe_3O_4\ NP)_{n=5-20}$, the $(rGO-SO_3^-/cationic\ Fe_3O_4\ NP)_{20}$, and the $(rGO-NH_3^+/rGO-SO_3^-)_{20}$ electrodes at a scan rate of 10 mV·s^{-1}. (d) CVs of the $(rGO-SO_3^-/OA-Fe_3O_4\ NP)_{20}$ electrode as a function of scan rate (5 to 100 mV·s^{-1}). (e) Nyquist plots of the $(rGO-SO_3^-/OA-Fe_3O_4\ NP)_n$ and $(rGO-NH_3^+/rGO-SO_3^-)_n$ electrodes. Inset indicates the high-frequency region. (f) Long-cycle performance of the $(rGO-SO_3^-/OA-Fe_3O_4\ NP)_{20}$ multilayer electrode at a scan rate of 100 mV·s^{-1}. In these cases, the solution concentrations of $rGO-SO_3^-$, $rGO-NH_3^+$, $OA-Fe_3O_4$ NP, and cationic Fe_3O_4 NP were adjusted to be approximately 0.5, 0.5, 10, and 10 mg·mL^{-1}, respectively.

soluble PSS (or toluene-dispersible $OA-Fe_3O_4$ NPs) (see Experimental Details in Supporting Information), which can play a role in decreasing the amount of PSS and $OA-Fe_3O_4$ NPs adsorbed onto the colloidal substrates. In the case of flat substrates, drying procedures were performed after a deposition/washing process of the respective functional components. Although the bilayer thickness analyzed by dynamic light scattering (DLS) was measured to be approximately 14.3 nm (see Supporting Information, Figure

S9), the interpretation of DLS data may involve the interplay of various factors such as electroviscosity, surface roughness, and shape irregularity,[81] which are believed to be responsible for the large size differences between DLS and SEM.

Although the amphiphilic LbL assembly resulted in a relatively low amount of functional components being adsorbed on the colloidal substrates compared to the flat substrates, this approach had a notable advantage for functional colloids: it allows for reversible phase transfer. Recently, our group

reported that a ligand exchange LbL assembly of neutral amine (NH_2)-functionalized dendrimers (NH_2−dendrimer) in alcohol and OA−Fe_3O_4 NPs in toluene can allow for reversible phase transfer of functional silica colloids between aqueous and toluene phases.[36] However, these colloids should be preferentially dispersed in an alcohol by coating with hydrogen-bonded layers, such as poly(acrylic acid) (PAA), before the phase transfer from water to toluene. As a result, the previously reported approach requires complex and careful steps for the preparation of colloids that allow for reversible phase transfer. Additionally, the NH_2-functionalized polymers used for LbL-assembled colloids in organic media were mainly limited to spherical-type polymers, such as dendrimer or block copolymer micelles, to avoid colloidal aggregation via polymer-chain-induced bridging effects. For example, when multilayers (i.e., [poly(ethylene imine) (PEI)/OA−Fe_3O_4 NP]$_n$) are deposited onto SiO_2 colloids using a linear NH_2-polymer, such as PEI (M_w, ∼1800), the outermost PEI layer-coated colloids aggregated in alcohol after the deposition of only 2 bilayers ($n = 2$). In contrast, the amphiphilic LbL approach allows for the reversible phase transfer of colloids between aqueous and nonpolar media through a direct assembly of PE and hydrophobic NPs without the insertion of an additional polymer layer. Furthermore, the colloids coated with a PSS layer were highly dispersible in aqueous media because of the strong electrostatic repulsion among the anionic-PSS-coated colloids. The dispersion stability of the amphiphilic LbL-assembled colloids in aqueous and nonpolar media can be maintained for over 1 week despite an increase in the number of layers up to 10.

Although polymers containing SO_3^- groups cannot be LbL-assembled using tetraoctylammonium bromide (TOABr)−Au (or, e.g., ethylamine−Fe_3O_4, −Au, or −TiO_2 NPs) with a strong affinity between the ammonium (or amine) group and the surface of the metal (or metal oxide) NP, a variety of metal or metal oxide NPs have been now developed using OA ligands,[42,43,58−60] and these NPs in various organic media (see the Supporting Information, Figure S10) can also be LbL-assembled with various SO_3^--polymers, such as semiconducting PEDOT:PSS (see Supporting Information, Figure S11), as well as insulating PSS (see Supporting Information, Figure S12). Moreover, considering that a high dispersion of colloids in different physical and chemical environments is required for many colloidal applications, our results suggest that amphiphilic LbL assembly could be effectively applied to the development of functional colloids, such as magnetically retrievable catalytic or conductive colloids used in aqueous and nonpolar media.

To further demonstrate the effectiveness and practicability of our approach, we fabricated amphiphilic LbL-assembled multilayer films composed of OA−Fe_3O_4 NPs and water-soluble rGO−$SO_3^{-61,62}$ instead of the SO_3^--functionalized polymers (see Supporting Information, Figure S13) and investigated the possibility that they can be used as super-capacitor electrodes with high performance. First, the high interaction affinity between the SO_3^- groups of the rGO sheets and OA−Fe_3O_4 NPs could be confirmed using the phase transfer method (see Supporting Information, Figure S14). These phenomena show that rGO−SO_3^- dispersed in water can be effectively LbL-assembled with OA−Fe_3O_4 NPs in nonpolar media such as toluene or hexane. However, the pH-related adsorption behavior of rGO−SO_3^- containing strong electrolyte groups is slightly different from that of PSS. Although the pH of the PSS solution has little effect on the

amount of PSS and next layer components (i.e., OA−Fe_3O_4 NP) adsorbed onto the amphiphilic LbL-assembled PSS/OA−Fe_3O_4 NP multilayers, the pH of the rGO−SO_3^- solution in the rGO−SO_3^-/OA−Fe_3O_4 NP multilayer system does exert a slight influence on the amount of rGO−SO_3^- and OA−Fe_3O_4 NPs adsorbed. rGO−SO_3^-, which is prepared through sulfonation with the aryl diazonium salt of sulfanilic acid,[61] still contains unsulfonated groups, such as carboxylic acid or hydroxyl. The presence of residual carboxylic acid within the rGO−SO_3^- can easily be detected by FTIR. As shown in the Supporting Information (Figure S15a), the absorbance peaks at 1416 and 1720 cm^{-1} in the FTIR spectrum of rGO−SO_3^- represent the symmetrical stretching of carboxylate (−COO^-) and the C═O stretching peak of carboxylic acid (−COOH) groups, respectively. In this case, the symmetrical stretching peak of the −COO^- group was investigated because the asymmetric stretching peak at 1520 cm^{-1} overlapped with the broad graphene domain peak at 1600 cm^{-1}. The charge density of rGO−SO_3^- was additionally increased due to the conversion from uncharged to charged carboxylic acid groups upon increasing the solution pH from 3 to 9, which affected the amounts of rGO−SO_3^-, and the next layer of OA−Fe_3O_4 NPs adsorbed (see Supporting Information, Figure S15b).

Figure 5a displays the bilayer number (or film thickness)-dependent cyclic voltammetry (CV) data of (rGO−SO_3^-/OA−Fe_3O_4 NP)$_n$ electrodes in 0.1 M Na_2SO_3 at a scan rate of 10 mV·s^{-1}. In this case, the thickness per bilayer was measured to be approximately 7.1 nm (see the Supporting Information, Figure S16), and the geometric current (mA·cm^{-2}) was found to increase with an increasing bilayer number of multilayers. However, the current density (mA·cm^{-3}) and the volumetric capacitance (F·cm^{-3}) of the multilayer electrodes were almost independent of bilayer number because the adsorbed amount per rGO−SO_3^-/OA−Fe_3O_4 NP bilayer was regular (see Supporting Information, Figure S17).

Figure 5b presents the CV data for (rGO−SO_3^-/OA−Fe_3O_4 NP)$_{20}$, (rGO−SO_3^-/cationic Fe_3O_4 NP)$_{20}$, and (rGO−SO_3^-/rGO−NH_3^+)$_{20}$ electrodes at a scan rate of 10 mV·s^{-1}. The CV curve of the electrostatically LbL-assembled (rGO−SO_3^-/rGO−NH_3^+)$_{20}$ electrode exhibited a rectangular shape with a relatively low current level in a potential range of −0.9 to +0.1 V, which is characteristic of double-layer capacitance.[62,63,82] However, for the (rGO−SO_3^-/OA−Fe_3O_4 NP)$_{20}$ electrode, the lack of symmetry in the redox peak curve was mainly due to the contribution of pseudocapacitive OA−Fe_3O_4 NPs to the total capacitance. As reported, the redox behavior of solution blending-based nanocomposite electrodes composed of Fe_3O_4 NPs and carbon nanofibers is mainly due to the redox reactions between the Fe^{II} and Fe^{III} of the inserted Fe_3O_4 NPs, as well as the surface redox reactions of sulfur (in the form of sulfate and sulfite anions) in an electrolyte solution.[83,84]

In this case, the volumetric current densities (in mA·cm^{-3}) and CV curve area of the (rGO−SO_3^-/OA−Fe_3O_4 NP)$_{20}$ electrode were higher and larger than those of the (rGO−SO_3^-/cationic Fe_3O_4)$_{20}$ and (rGO−SO_3^-/rGO−NH_3^+)$_{20}$ electrodes, respectively (a detailed synthetic procedure for cationic Fe_3O_4 NPs is given in the Supporting Information). Although the (rGO−SO_3^-/cationic Fe_3O_4)$_n$ electrode also displayed pseudocapacitive features in the CV curves, its pseudocapacitive performance was considerably lower than that of the (rGO−SO_3^-/OA−Fe_3O_4)$_{20}$ electrode due to the low packing density of the cationic Fe_3O_4 NPs. Additionally, the total integrated charge density (in mC·cm^{-2}) of the (rGO−SO_3^-/OA−Fe_3O_4

$NP)_n$ electrode increased nearly linearly with the number of bilayers (or film thickness) of the multilayer electrodes, implying that the total electrode capacity can be further increased by increasing the bilayer number (Figure 5c). As a result, the $(rGO-SO_3^-/OA-Fe_3O_4\ NP)_{20}$, $(rGO-SO_3^-/$ cationic $Fe_3O_4\ NP)_{20}$, and $(rGO-SO_3^-/rGO-NH_3^+)_{20}$ electrodes displayed volumetric capacitances of 280, 154, and 91 F·cm^{-3} at 10 mV·s^{-1}, respectively.

The $(rGO-SO_3^-/OA-Fe_3O_4\ NP)_n$ electrode also displayed a good rate capability when increasing the scan rate from 5 to 100 mV·s^{-1}, which suggested that these multilayers exhibited rapid charge transfer and ion diffusion (Figure 5d). Nyquist plots were obtained from electrochemical impedance spectroscopy (EIS) measurement by applying an AC voltage with a magnitude of 50 mV in a frequency range from 100 kHz to 0.1 Hz (Figure 5e). In the low-frequency region, the $(rGO-SO_3^-/OA-Fe_3O_4\ NP)_n$ and $(rGO-\ NH_3^+/rGO-SO_3^-)_n$ electrodes displayed similar capacitive behavior, where a tendency to lie parallel with the imaginary axis (Z'') represents an ideal capacitor.[82] However, in the extremely high-frequency region (in the inset), the semicircle, which corresponds to the charge-transfer resistance originating from the redox reaction of the $OA-Fe_3O_4$ NPs adsorbed onto the $rGO-SO_3^-$ nanosheets, was observed for the $(rGO-SO_3^-/OA-Fe_3O_4\ NP)_{20}$ electrode but not for the $(rGO-NH_3^+/rGO-SO_3^-)_{20}$ electrode. Because of the densely packed $OA-Fe_3O_4$ NPs on the $rGO-SO_3^-$ nanosheets, the intercept of the equivalent-series resistance (ESR) (i.e., the sum of the total resistances, including the ionic resistance of electrolyte, the electronic resistance of $OA-Fe_3O_4$ NPs, and the contact resistance of active material/current collector) with the real axis (Z') for the $(rGO-SO_3^-/OA-Fe_3O_4)_{20}$ electrode (138 Ω) was higher than that for the $(rGO-NH_3^+/rGO-SO_3^-)_{20}$ electrode (53 Ω). We also investigated the changes in the galvanostatic charge–discharge curves of the $(rGO-SO_3^-/OA-Fe_3O_4\ NP)_{20}$ film electrodes as the current density was increased from 1 to 6.5 A·g^{-1} (see Supporting Information, Figure S18a). In this case, the inclined regions (or minor charge–discharge plateau) in the charging potential window ranging from −0.8 to −0.6 V and the discharging potential window ranging from −0.7 to −0.9 V exhibited the redox reactions, which corresponded to the CV curve redox peaks of the $(rGO-SO_3^-/OA-Fe_3O_4\ NP)_{20}$ film electrode in Figure 5a. More specifically, at values greater than −0.6 V, the time dependence of the potential is linear, implying pure double-layer capacitance behavior from the charge separation at the electrode−electrolyte interface. In contrast, at values less than −0.6 V, the time dependence of the potential was nonlinear due to the pseudocapacitive behavior of densely packed $OA-Fe_3O_4$ NPs within the electrodes. These phenomena are a stark contrast to the linear time-dependent behavior of the electrostatic $(rGO-SO_3^-/rGO-NH_3^+)_{20}$ film electrode without cationic Fe_3O_4 or $OA-Fe_3O_4$ NPs (see Supporting Information, Figure S18b). Furthermore, the long-term cycling performance of the $(rGO-SO_3^-/OA-Fe_3O_4\ NP)_{20}$ electrode at a scan rate of 100 mV·s^{-1} for 1000 cycles is shown in Figure 5f. After 1000 cycles, only a 7% loss of the initial capacitance was observed, implying good electrochemical stability of the electrode. Although a variety of ultrathin-film-type supercapacitor electrodes based on carbon-based materials/pseudocapacitive NPs or carbon/carbon-based materials have been investigated by many research groups,[84−87] these materials have mainly been prepared using the electrostatic attractions between neighboring materials. Therefore, the

formed electrodes exhibited relatively low mass densities of pseudocapacitive materials due to the electrostatic charge repulsions among the charged pseudocapacitive NPs, which induced relatively low volumetric capacitance and operation stability. For example, Byon et al. reported the electrostatically LbL-assembled MWCNT/rGO thin-film electrodes with a high volumetric capacitance of 160 F·cm^{-3}.[85] Hyder et al. demonstrated that electrostatic LbL film electrodes composed of cationic TiO_2 NPs and anionic MWCNTs exhibited a maximum capacitance of 228 ± 19 F·cm^{-3} at a scan rate of 1 mV·s^{-1}.[86] Wu et al. reported chemically converted, graphene/polyaniline nanofiber composite electrodes prepared through ultrasonication and filtration. These composite electrodes exhibited a volumetric capacitance of 160 F·cm^{-3} and maintained 71% of the initial capacitance after 800 cycles.[87] Additionally, Liu et al. generated quasi-cubic Fe_3O_4@rGO composite electrodes by an electrostatic assembly process between cationic $Fe(OH)_3$ NPs and anionic GO sheets as supercapacitor electrodes.[88] These electrodes exhibited a specific capacitance of 216.7 F·g^{-1} and maintained approximately 85% of its initial capacitance after 1000 cycles.

In contrast, the high-energy storage performance (i.e., 280 F·cm^{-3} at 10 mV·s^{-1}, 93% retention of initial capacitance after 1000 cycles) of the $(rGO-SO_3^-/OA-Fe_3O_4\ NP)_n$ electrodes prepared in our approach was mainly due to the formation of a densely packed $OA-Fe_3O_4$ NP array on the $rGO-SO_3^-$ layer with good access to the electrolyte electrons and ions

4. CONCLUSIONS

In conclusion, we successfully prepared nanocomposite multilayers based on a variety of hydrophobic NPs (metal or metal oxide NPs) and hydrophilic materials using amphiphilic LbL assembly in nonpolar and aqueous solvents. The main driving force for the buildup of multilayers is the ligand exchange reaction between the carboxylic acid groups of OA ligands loosely bound to metal or metal oxide NPs in various organic media, including nonpolar (e.g., toluene or hexane) or polar organic (e.g., THF or chloroform) solvent and the strong acid groups (i.e, stronger acid groups than carboxylic acid groups), such as SO_3^- and PO_3^{2-} of hydrophilic materials, in aqueous media. These results imply that OA-stabilized NPs can be easily LbL-assembled with hydrophilic materials containing stronger acid groups than the carboxylic acid groups of the OA ligands irrespective of solvent polarity and the type of metal or metal oxide NP. We also demonstrated that our strategy allows the adsorption of densely packed NP arrays on SO_3^--based material layers and that their packing density can be easily controlled by the ionic strength of the preadsorbed charged layer. These results imply that the amphiphilic LbL assembly can exploit the major advantages of aqueous and organic solvent-based LbL assemblies. Furthermore, our approach can be effectively used for the fabrication of high-performance energy storage devices from amphiphilic LbL nanocomposites composed of $rGO-SO_3^-$ and $OA-Fe_3O_4$ NPs. Because the amphiphilic LbL assemblies can be easily incorporated into a variety of functional materials within ultrathin films irrespective of their hydrophilicity or hydrophobicity, we believe that our approach can provide the basis for the design and exploitation of various potential applications.

■ ASSOCIATED CONTENT

Ⓢ Supporting Information

Experimental details, FTIR spectra, UV−vis spectra, QCM data, SQUID data, DLS data, Raman spectra, HR-TEM results, CV curves, Galvanostatic charge−discharge curves. This material is available free of charge via the Internet at http://pubs.acs.org.

■ AUTHOR INFORMATION

Corresponding Author

jinhan71@korea.ac.kr

Author Contributions

§These authors equally contributed to this work.

Notes

The authors declare no competing financial interest.

■ ACKNOWLEDGMENTS

■ REFERENCES

(1) Decher, G. *Science* **1997**, *277*, 1232.
(2) Balazs, A. C.; Emrick, T.; Russell, T. P. *Science* **2006**, *314*, 1107.
(3) Gong, J.; Li, G.; Tang, Z. *Nano Today* **2012**, *7*, 564.
(4) Podsiadlo, P.; Kaushik, A. K.; Arruda, E. M.; Waas, A. M.; Shim, B. S.; Xu, J. D.; Nandivada, H.; Pumplin, B. G.; Lahann, J.; Ramamoorthy, A.; Kotov, N. A. *Science* **2007**, *318*, 80.
(5) Ji, Q.; Honma, I.; Paek, S.-M.; Akada, M.; Hill, J. P.; Vinu, A.; Ariga, K. *Angew. Chem., Int. Ed.* **2010**, *49*, 9737.
(6) Caruso, F.; Caruso, R. A.; Möhwald, H. *Science* **1998**, *282*, 1111.
(7) Lee, S. W.; Kim, J.; Chen, S.; Hammond, P. T.; Shao-Horn, Y. *ACS Nano* **2010**, *4*, 3889.
(8) Xiao, F.-X.; Miao, J.; Liu, B. *J. Am. Chem. Soc.* **2014**, *136*, 1559.
(9) Qin, B.; Chen, H.; Liang, H.; Fu, L.; Liu, X.; Qiu, X.; Liu, S.; Song, R.; Tang, Z. *J. Am. Chem. Soc.* **2010**, *132*, 2886.
(10) Malile, B.; Chen, J. I. L. *J. Am. Chem. Soc.* **2013**, *135*, 16042.
(11) Richardson, J. J.; Ejima, H.; Lörcher, S. L.; Liang, K.; Senn, P.; Cui, J.; Caruso, F. *Angew. Chem., Int. Ed.* **2013**, *52*, 6455.
(12) Suda, M.; Einaga, Y. *Angew. Chem., Int. Ed.* **2009**, *48*, 1754.
(13) Liu, S.; Tang, Z. *J. Mater. Chem.* **2010**, *20*, 24.
(14) Tang, H.; Yin, H.; Wang, J.; Yang, N.; Wang, D.; Tang, Z. *Angew. Chem., Int. Ed.* **2013**, *52*, 5585.
(15) Gu, H.; Bi, L.; Wang, N.; Liu, S.; Tang, Z. *Chem. Sci.* **2013**, *4*, 4371.
(16) Warren, S. C.; Messina, L. C.; Slaughter, L. S.; Kamperman, M.; Zhou, Q.; Gruner, S. M.; DiSalvo, F. J.; Wiesner, U. *Science* **2008**, *320*, 1748.
(17) Boal, A. K.; Ilhan, F.; DeRouchey, J. E.; Thurn-Albrecht, T.; Russell, T. P.; Rotello, V. M. *Nature* **2000**, *404*, 746.
(18) Uzun, O.; Frankamp, B. L.; Sanyal, A.; Rotello, V. M. *Chem. Mater.* **2006**, *18*, 5404.
(19) Li, M.; Ishihara, S.; Akada, M.; Liao, M.; Sang, L.; Hill, J. P.; Krishnan, V.; Ma, Y.; Ariga, K. *J. Am. Chem. Soc.* **2011**, *133*, 7348.
(20) So, M. C.; Jin, S.; Son, H.-J.; Wiederrecht, G. P.; Farha, O. K.; Hupp, J. T. *J. Am. Chem. Soc.* **2013**, *135*, 15698.
(21) Kaschak, D. M.; Lean, J. T.; Waraksa, C. C.; Saupe, G. B.; Usami, H.; Mallouk, T. E. *J. Am. Chem. Soc.* **1999**, *121*, 3435.
(22) Li, H.; Pang, S.; Wu, S.; Feng, X.; Müllen, K.; Bubeck, C. *J. Am. Chem. Soc.* **2011**, *133*, 9423.
(23) Iler, R. K. *J. Colloid Inter. Sci.* **1966**, *21*, 569.
(24) Jiang, C.; Markutsya, S.; Pikus, Y.; Tsukruk, V. V. *Nat. Mater.* **2004**, *3*, 721.
(25) Tettey, K. E.; Yee, M. Q.; Lee, D. *ACS Appl. Mater. Interfaces* **2010**, *2*, 2646.
(26) Zhao, N.; Shi, F.; Wang, Z.; Zhang, X. *Langmuir* **2005**, *21*, 4713.
(27) Crespo−Biel, O.; Dordi, B.; Reinhoudt, D. N.; Huskens, J. *J. Am. Chem. Soc.* **2005**, *127*, 7594.
(28) Cassagneau, T.; Mallouk, T. E.; Fendler, J. H. *J. Am. Chem. Soc.* **1998**, *120*, 7848.
(29) Wang, T. C.; Rubner, M. F.; Cohen, R. E. *Langmuir* **2002**, *18*, 3370.
(30) Zhai, L.; Cebeci, F. C.; Cohen, R. E.; Rubner, M. F. *Nano Lett.* **2004**, *4*, 1349.
(31) Lee, B.; Kim, Y.; Lee, S.; Kim, Y. S.; Wang, D.; Cho, J. *Angew. Chem., Int. Ed.* **2010**, *49*, 359.
(32) Yoon, M.; Kim, Y.; Cho, J. *ACS Nano* **2011**, *5*, 5417.
(33) Zhang, F.; Srinivasan, M. P. *Langmuir* **2007**, *23*, 10102.
(34) Krasteva, N.; Besnard, I.; Guse, B.; Bauer, R. E.; Mullen, K.; Yasuda, A.; Vossmeyer, T. *Nano Lett.* **2002**, *2*, 551.
(35) Ko, Y.; Baek, H.; Kim, Y.; Yoon, M.; Cho, J. *ACS Nano* **2013**, *7*, 143.
(36) Yoon, M.; Choi, J.; Cho, J. *Chem. Mater.* **2013**, *25*, 1735.
(37) Cho, J.; Caruso, F. *Macromolecules* **2003**, *36*, 2845.
(38) Hao, E.; Lian, T. *Langmuir* **2000**, *16*, 7879.
(39) Zhang, H.; Fu, Y.; Wang, D.; Wang, L.; Wang, Z.; Zhang, X. *Langmuir* **2003**, *19*, 8497.
(40) Tetty, K. E.; Yee, M. Q.; Lee, D. *Langmuir* **2010**, *26*, 9974.
(41) Huang, H.-C.; Zacharia, N. S. *ACS Macro Lett.* **2012**, *1*, 209.
(42) Sun, S.; Zeng, H. *J. Am. Chem. Soc.* **2002**, *124*, 8204.
(43) Wang, X.; Zhuang, J.; Peng, Q.; Li, Y. *Nature* **2005**, *437*, 121.
(44) Gittins, D. I.; Susha, A. S.; Schoeler, B.; Caruso, F. *Adv. Mater.* **2002**, *14*, 508.
(45) Depalo, N.; Comparelli, R.; Huskens, J.; Ludden, M. J. W.; Perl, A.; Agostiano, A.; Striccoli, M.; Curri, M. L. *Langmuir* **2012**, *28*, 8711.
(46) Hong, J.; Bae, W. K.; Lee, H.; Oh, S.; Char, K.; Caruso, F.; Cho, J. *Adv. Mater.* **2007**, *19*, 4364.
(47) Kong, H.; Luo, P.; Gao, C.; Yan, D. *Polymer* **2005**, *46*, 2472.
(48) Stankovich, S.; Dikin, D. A.; Dommett, G. H. B.; Kohlhaas, K. M.; Zimney, E. J.; Stach, E. A.; Piner, R. D.; Nguyen, S. T.; Ruoff, R. S. *Nature* **2006**, *442*, 282.
(49) Xu, Y. F.; Liu, Z.; Zhang, X.; Wang, Y.; Tian, J.; Huang, Y.; Ma, Y.; Zhang, X.; Chen, Y. *Adv. Mater.* **2009**, *21*, 1275.
(50) Tang, X.-Z.; Li, W.; Yu, Z.-Z.; Rafiee, M. A.; Rafiee, J.; Yavari, F.; Koratkar, N. *Carbon* **2011**, *49*, 1258.
(51) Dong, X.; Wang, L.; Wang, D.; Li, C.; Jin, J. *Langmuir* **2012**, *28*, 293.
(52) Yang, M.; Hou, Y.; Kotov, N. A. *Nano Today* **2012**, *7*, 430.
(53) Medintz, I. L.; Uyeda, H. T.; Goldman, E. R.; Mattoussi, H. *Nat. Mater.* **2005**, *4*, 435.
(54) Bagaria, H. G.; Ada, E. T.; Shamsuzzoha, M.; Nikles, D. E.; Johnson, D. T. *Langmuir* **2006**, *22*, 7732.
(55) Lin, W.; Fritz, K.; Guerin, G.; Bardajee, G. R.; Hinds, S.; Sukhovatkin, V.; Sargent, E. H.; Scholes, G. D.; Winnik, M. A. *Langmuir* **2008**, *24*, 8215.
(56) Wu, C.-K.; Hultman, K. L.; O'Brien, S.; Koberstein, J. T. *J. Am. Chem. Soc.* **2008**, *130*, 3516.
(57) Schlenoff, J. B.; Dubas, S. T.; Farhat, T. *Langmuir* **2000**, *16*, 9968.
(58) Lin, X. Z.; Teng, X.; Yang, H. *Langmuir* **2003**, *19*, 10081.
(59) Sun, S.; Zeng, H.; Robinson, D. B.; Raoux, S.; Rice, P. M.; Wang, S. X.; Li, G. *J. Am. Chem. Soc.* **2004**, *126*, 273.
(60) Pan, D.; Zhao, N.; Wang, Q.; Jiang, S.; Ji, X.; An, L. *Adv. Mater.* **2005**, *17*, 1991.
(61) Si, Y.; Samulski, E. T. *Nano Lett.* **2008**, *8*, 1679.
(62) Xiong, Z.; Gu, T.; Wang, X. *Langmuir* **2014**, *30*, 522.
(63) Lee, S. W.; Kim, B.-S.; Chen, S.; Shao-Horn, Yang; Hammond, P. T. *J. Am. Chem. Soc.* **2009**, *131*, 671.
(64) Zhang, L.; He, R.; Gu, H.-C. *Appl. Surf. Sci.* **2006**, *253*, 2611.
(65) Sun, S. *Adv. Mater.* **2006**, *18*, 393.

(66) Yee, C.; Kataby, G.; Ulman, A.; Prozorov, T.; White, H.; King, A.; Rafailovich, M.; Sokolov, J.; Gedanken, A. *Langmuir* **1999**, *15*, 7111.

(67) Kim, J.; Kim, H.; Kim, G.; Back, H.; Lee, K. *ACS Appl. Mater. Interfaces* **2014**, *6*, 951.

(68) Polito, L.; Colombo, M.; Monti, D.; Melato, S.; Caneva, E.; Prosperi, D. *J. Am. Chem. Soc.* **2008**, *130*, 12712.

(69) Schlenoff, J. B.; Ly, H.; Li, M. *J. Am. Chem. Soc.* **1988**, *120*, 7626.

(70) Cho, J.; Caruso, F. *Chem. Mater.* **2005**, *17*, 4547.

(71) Liang, Z.; Susha, A.; Caruso, F. *Chem. Mater.* **2003**, *15*, 3176.

(72) Park, J.; An, K.; Hwang, Y.; Park, J.-E.; Noh, H.-J.; Kim, J.-Y.; Park, J.-H.; Hwang, N.-M.; Hyeon, T. *Nat. Mater.* **2004**, *3*, 891.

(73) Poddar, P.; Telem-Shafir, T.; Fried, T.; Markovich, G. *Phys. Rev. B* **2002**, *66*, 060403.

(74) Cheong, S.; Kim, Y.; Kwon, T.; Kim, B. J.; Cho, J. *Nanoscale* **2013**, *5*, 12356.

(75) Bernal, J. D.; Mason, J. *Nature* **1960**, *188*, 910.

(76) Grabar, K. C.; Allison, K. J.; Baker, B. E.; Bright, R. M.; Brown, K. R.; Freeman, R. G.; Fox, A. P.; Keating, C. D.; Musick, M. D.; Natan, M. J. *Langmuir* **1996**, *12*, 2353.

(77) Schmitt, J.; Decher, G.; Dressick, W. J.; Brandow, S. L.; Geer, R. E.; Shashidhar, R.; Calvert, J. M. *Adv. Mater.* **1997**, *9*, 61.

(78) Xi, Q.; Chen, X.; Evans, D. G.; Yang, W. *Langmuir* **2012**, *28*, 9885.

(79) Yoo, D.; Shiratori, S. S.; Rubner, M. F. *Macromolecules* **1998**, *31*, 4309.

(80) Cho, J.; Char, K. *Langmuir* **2004**, *20*, 4011.

(81) Gittings, M. R.; Saville, D. A. *Colloids Surf., A* **1998**, *141*, 111.

(82) Stoller, M. D.; Park, S.; Zhu, Y.; An, J.; Ruoff, R. S. *Nano Lett.* **2008**, *8*, 3498.

(83) Mu, J.; Chen, B.; Guo, Z.; Zhang, M.; Zhang, P.; Shao, C.; Liu, Y. *Nanoscale* **2011**, *3*, 5034.

(84) Wu, N.-L.; Wang, S.-Y.; Han, C.-Y.; Wu, D.-S.; Shiue, L.-R. *J. Power Source* **2003**, *113*, 173.

(85) Byon, H. R.; Lee, S. W.; Chen, S.; Hammond, P. T.; Shao-Horn, Y. *Carbon* **2011**, *49*, 457.

(86) Hyder, M. N.; Gallant, B. N.; Shah, N. J.; Shao-Horn, Y. *Nano Lett.* **2013**, *13*, 4610.

(87) Wu, Q.; Xu, Y.; Yao, Z.; Liu, A.; Shi, G. *ACS Nano* **2010**, *4*, 1963.

(88) Liu, T.; Zhang, X.; Li, B.; Ding, J.; Liu, Y.; Li, G.; Meng, X.; Cai, Q.; Zhang, J. *RSC Adv.* **2014**, *4*, 50765.